Journal of Zhejiang University-SCIENCE A (Applied Physics & Engineering)
ISSN 1673-565X (Print); ISSN 1862-1775 (Online)
www.jzus.zju.edu.cn; link.springer.com
E-mail: jzus_a@zju.edu.cn

Adsorption of tetrodotoxin by flexible shape-memory polymers synthesized from silica-stabilized Pickering high internal phase emulsion*#

Hong-xiang OU†[1,2], Chen-xia GONG[1], Hong-lai XUE[1,2], Dong-sheng ZHOU[1], Kai-jia LI[1], Shu-cheng LIU[3]

[1]*School of Environmental and Safety Engineering, Changzhou University, Changzhou 213164, China*

[2]*Institute of Public Safety and Emergency Management, Changzhou University, Changzhou 213164, China*

[3]*School of Chemistry and Chemical Engineering, Jiangsu University, Zhenjiang 212013, China*

†E-mail: ouhongxiang@cczu.edu.cn

Received Oct. 3, 2020; Revision accepted Feb. 14, 2021; Crosschecked Sept. 27, 2021

Abstract: Flexible shape-memory polymers were synthesized by Pickering high internal phase emulsion (HIPE) polymerization and used to adsorb and separate tetrodotoxin (TTX) from an aqueous solution. SiO_2 nanoparticles were used to stabilize the Pickering oil-in-water (O/W) HIPEs. We introduced imidazolium-modified bromobutyl rubber (IBR) with excellent mechanical properties and high viscosity into the emulsion system as the shape-memory monomer. The properties, such as shape memory and morphology, were characterized by various methods, and batches of static adsorption experiments were conducted to analyze the adsorption performance of SiO_2@IBR on TTX. The characterization revealed that the SiO_2@IBR had a porous structure and good shape memory. Thus, the combination of SiO_2 particles and IBR prevented shedding of SiO_2 and enhanced the mechanical and adsorption properties of SiO_2@IBR. The results of the adsorption experiments indicated that the SiO_2@IBR had good adsorption of TTX. Both the Langmuir and Freundlich models fitted the isothermal adsorption experiment process. The TTX adsorption capacity of SiO_2@IBR was about 290.44 mg/g at 308 K. The fitting results of the pseudo-first-order and pseudo-second-order kinetic models showed that the adsorption process involved both chemical bonding and physical adsorption. After 10 adsorption and desorption experiments, the adsorption capacity of SiO_2@IBR decreased less than 0.03%, indicating that it had good adsorption and regeneration performance.

Key words: Tetrodotoxin (TTX); SiO_2; Imidazolium-modified bromobutyl rubber (IBR); Pickering high internal phase emulsion (HIPE); Adsorption

https://doi.org/10.1631/jzus.A2000433 **CLC number:** R284.2

1 Introduction

Tetrodotoxin (TTX) is an alkaloid existing in puffer fish and other organisms. It is an amino perhydroquinazoline compound with a complex structure (Ohyabu et al., 2003; Pichierri, 2016; Deniz Akbora et al., 2020). A large number of studies have shown that a small amount of TTX has pharmacological effects of sedation, analgesia, and local anesthesia, and it has a major role in the treatment of epilepsy, arrhythmia, renal failure, and drug addiction (Song et al., 2011; Hagen et al., 2017; Hong et al., 2019). Because of its unique physiologically active functions and extraordinary pharmacological effects, TTX has great medical development value. However, in the production processing of puffer fish, their highly toxic parts are often treated as waste, which not

* Project supported by the National Natural Science Foundation of China (No.21878026), the Postgraduate Research & Practice Innovation Program of Jiangsu Province (No. KYCX19_1798), the Jiangsu Province University Blue Project, and the Project of Higher Education Reform in Jiangsu Province (No. 2019JSJG022), China

Electronic supplementary materials: The online version of this article (https://doi.org/10.1631/jzus.A2000433) contains supplementary materials, which are available to authorized users

ORCID: Hong-xiang OU, https://orcid.org/0000-0001-8329-8014

only wastes resources, but also brings certain potential hazards (Yang et al., 2019; Zhang et al., 2019). Therefore, the development of simple and efficient TTX separation and purification methods has great scientific, social, and economic value.

There have been some reports on the extraction and purification methods for TTX. The raw materials are first roughly extracted by the water bath method and ultrasonic-assisted method. Then, the crude extract is separated and purified to obtain relatively pure TTX (Huang et al., 2011; Chen et al., 2014). However, most of the TTX production methods currently employed stop at the rough extraction stage because the purification and refining process is quite complicated, which limits the large-scale production and application of high-purity TTX. The adsorption method is an alternative that is widely applied to separation and purification with the advantages of simple operation and low cost (Das et al., 2018; Peng et al., 2019; Fan et al., 2020). Novel adsorption materials with better adsorption capacity are of great significance for TTX purification and its application in clinical medicine.

SiO_2 nanoparticles are often used for adsorption and separation due to large specific surface area, and strong surface adsorption capacity (Tanzifi et al., 2018a; Chen et al., 2019). However, since SiO_2 nanoparticles are only tens of nanometers in size, the recycling and reprocessing of the powdered material is not easy, making it difficult to separate and reuse. Pickering high internal phase emulsion (HIPE) polymerization is a simple and environmentally friendly method for preparing macroporous adsorbent materials (Azhar et al., 2019; Lu et al., 2019). Using this technique and applying SiO_2 nanoparticles as the stabilizer for the emulsions, the SiO_2 nanoparticles can be successfully connected, which makes it convenient to collect them after adsorption. However, the flexibility of silica-based adsorbents prepared by Pickering HIPE polymerization is generally poor, and they are easily damaged during operations such as adsorption and desorption. Furthermore, their service lifetime is also reduced by use.

Common flexible materials which can be used for adsorption and separation include polyurethane foam, polypropylene fiber, and gel (Dupont et al., 2020; Li et al., 2020). They have the advantages of simple separation and adsorption operation, sturdiness, and ease of recycling. Yi et al. (2016) used HIPEs to prepare polypropylene gels for adsorption and recovery of Cu^{2+}. Wang QZ et al. (2020) prepared porous gelatin-based aerogels to adsorb and separate oils or organic solvents from water. However, these materials still have shortcomings, such as tunnels that collapse easily, and the structure is easily destroyed by external force. These problems hinder their repeated use in practical applications. Meanwhile, rubber has good mechanical properties and elasticity, can produce large deformation under a small external force, and can return to its original state after the external force is removed (Rattanasom et al., 2009; Segiet et al., 2020). Das et al. (2015) produced an imidazolium-modified bromobutyl rubber (IBR) that formed a cross-linked network by ionic association; the rubber matrix became highly viscoelastic. The properties of this ionically modified bromobutyl rubber were superior to those of conventionally cross-linked rubber and tensile strength up to 9 MPa at a fracture elongation of 1000% was obtained. If a modified rubber like this is appropriately added to an adsorption material to form a protective network, it gives the material a more stable structure and better mechanical properties.

Inspired by the above research, in this study, we fabricated SiO_2@IBR by Pickering oil-in-water (O/W) HIPE polymerization with SiO_2 nanoparticles as the stabilizer, and used it to adsorb and separate TTX from aqueous solutions. It is worth noting that the highly viscoelastic IBR was dispersed in the oil phase, and was uniformly distributed on the gap and surface of the polymers after polymerization, which resulted in polymers with good mechanical properties and shape-memory function.

Our expectation was that the polymers would swell like a sponge after absorbing the target from the solution. In addition, we predicted that the swollen polymers would be deformed when squeezed by an external force, so that the eluent in the channel would be squeezed out, and that the polymers would quickly return to their original state after removing the external force. This reversible "shape-memory" effect is very important for the adsorption and release of the captured target, and can simplify the adsorption regeneration process. We studied several aspects of

adsorption performance including isotherm data, kinetics, and adsorption regeneration. The polymers were characterized by methods such as scanning electron microscopy (SEM) and attenuated total reflectance-Fourier transform infrared spectroscopy (ATR-FTIR).

2 Experimental

2.1 Materials and methods

Bromobutyl rubber (BIIR, Bromine content 1.91% (in weight, the same below in this subsection)) was purchased from Sinopec Yanshan Petrochemical Company (Beijing, China). 1-butylimidazole ($C_7H_{12}N_2$, 98%), N,N'-methylenebisacrylamide (MBAA) ($C_7H_{10}N_2O_2$, 97%), acetic acid (CH_3COOH), and tetrodotoxin (TTX, $C_{11}H_{17}N_3O_8$, ≥99%) were purchased from Shanghai Aladdin Biochemical Technology Co., Ltd. (Shanghai, China). Acrylic acid (AA) ($C_3H_4O_2$, 98%), potassium persulfate (KPS) ($K_2S_2O_8$, 99.5%), and sodium hydroxide (NaOH, ≥96%) were purchased from Sinopharm Chemical Reagent Co., Ltd. (Shanghai, China). Monodispersed silica microspheres (SiO_2, 99.9%, 30 nm-sized) were purchased from Shanghai Macklin Biochemical Co., Ltd. (Shanghai, China). Petroleum ether (boiling point: 363–393 K) was purchased from Shanghai Lingfeng Chemical Reagent Co., Ltd. (Shanghai, China). Acetic acid and petroleum ether were of analytical grade. Deionized water was used in all experiments. All the reagents were used without any purification.

2.2 Preparation of SiO_2@IBR

2.2.1 Preparation of IBR

The preparation of IBR was based on Das et al. (2015). At a high temperature of 423 K, 50 g of BIIR and 1.89 g (2 mL) of 1-butylimidazole were added to an internal mixer (XM-1 L, Thermo fisher, USA) for curing experiments. The curing time was 10 min and the rotor speed was 60 r/min. In this way, the IBR was obtained.

2.2.2 Preparation of SiO_2@IBR

The processes for preparing the Pickering HIPEs and SiO_2@IBR are illustrated in Fig. 1.

First, 1.5 g of IBR was added to 50 mL of petroleum ether and left to stand for 10 d. On the 7th and 8th days, it was heated once for 5 h each time. Then, 7 mL of swelling liquid (without lumpy adhesion) was taken out and mixed with 5 mL of petroleum ether to obtain the oil phase. Second, 1 mL of AA, 0.0027 g of KPS, 0.0283 g of MBAA, and 0.28 g of SiO_2 nanoparticles were sequentially added to 3 mL of deionized water, and each material was uniformly dispersed in deionized water after 15 min of ultrasound. The IBR and petroleum ether mixture (12 mL) was gradually added dropwise into the water phase, and stirred with a glass rod for 20 min to form stable Pickering O/W HIPEs. Then, the emulsions were placed in an oven (101-2B, Hangzhou Hengyi Instrument Technology Co., Ltd., China) and polymerized at 85 °C for 12 h (the sample bottle was sealed to prevent evaporation). Finally, the samples were collected, washed with deionized water, and dried at 60 °C. In this way, SiO_2/imidazolium-modified bromobutyl rubber flexible shape-memory polymers (SiO_2@IBR) were obtained.

2.3 Characterization

2.3.1 Viscoelasticity and mechanical property tests of IBR

First, the IBR sample was cut into two pieces. Then, the two pieces were reassembled and the sample was allowed to sit. After 24 h of healing time, the sample was stretched to fracture.

2.3.2 Morphological characterization

The morphology of the Pickering O/W HIPEs was observed under an electron microscope (EM) (XSP-35-1600X, Phenix, China). The microstructure of SiO_2@IBR samples was inspected under a scanning electron microscope (SEM) (JSM-6360, JEOL, Japan) at 20 kV. Before the SEM test, the samples were coated with platinum (Pt).

2.3.3 FTIR analysis

FTIR spectroscopy of the samples was analyzed by an infrared spectrometer with a universal ATR accessory (ATR-FTIR) (Nicolet IS-50, Thermo fisher, USA). After subtracting the background, infrared spectra of the samples were recorded in the region of 4000 cm^{-1} to 400 cm^{-1}.

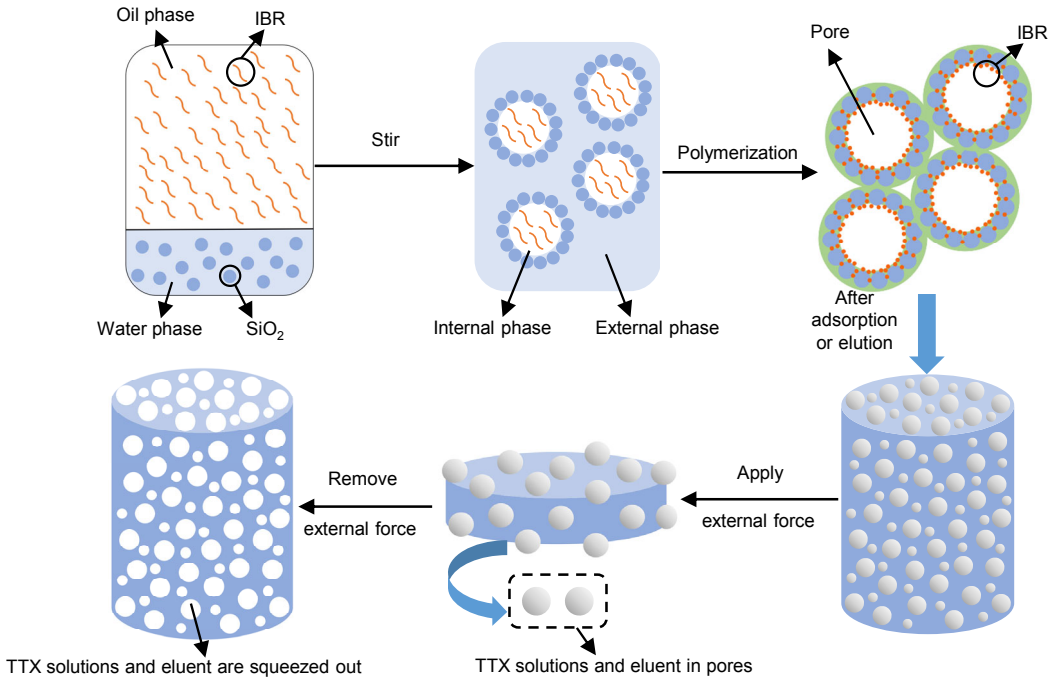

Fig. 1 Formation of SiO_2@IBR with macroporous structure and good flexibility derived from Pickering O/W HIPEs and shape-memory schematic

2.3.4 "Shape-memory" property test

The mechanical properties of the SiO_2@IBR sample were tested by a universal material testing machine (WDT-10, Kai Qiang Li, China). The YSM001-general compression test method was adopted, the test speed was set to 4 mm/min, and different maximum compression deformations (7.50, 13.50, 16.10 mm) were set to test the same sample three times.

2.3.5 Swelling property test

The swelling property of SiO_2@IBR was determined by calculating its water absorption rate. The samples (6 mg) were immersed in deionized water after drying to a constant weight, and left to sit at room temperature. At 5, 15, 30, 60, 120, 180, 360, 540, 720, and 1080 min, the samples were removed from the deionized water; their weights m_t (mg) were recorded immediately. The weight swelling rate (WS) of the SiO_2@IBR samples at time t (mg/mg) was calculated by (Cheng et al., 2019)

$$\mathrm{WS}=\frac{m_t-m_0}{m_0}, \tag{1}$$

where m_0 (mg) is the original weight of the samples, and m_t (mg) is the weight of the samples at time t.

2.4 Adsorption experiments

2.4.1 Adsorption kinetics

SiO_2@IBR polymers (3 mg) were added to 3 mL of TTX solution with initial concentration of 8 mg/L. Then the testing solution was shaken in a shaker (ZD-85A, Jintan Chengdong Xinrui Instrument Factory, China) at 308 K. At 5, 15, 30, 60, 120, 180, 360, and 720 min, the adsorbents were collected from the testing solution with tweezers, and squeezed until no solution could be expressed. After the testing solution was hydrolyzed with an alkaline treatment, the concentration of TTX at different times was measured by ultraviolet spectrophotometer (UV/VIS) (UV1901, Shanghai Xipu Instrument Co., Ltd., China) at a detection wavelength of 231 nm (Chen and Cheng, 1984; Kan and Guo, 2008). The adsorption capacity Q_t (mg/g) was calculated by (Wang B et al., 2020):

$$Q_t=\frac{(C_0-C_t)\times V}{W}, \tag{2}$$

where Q_t (mg/g) is the adsorption capacity of

SiO_2@IBR polymers on TTX at time t; C_0 (mg/L) is the initial concentration of TTX; C_t (mg/L) is the equilibrium adsorption concentration at time t; V (mL) is the volume of the TTX solution; W (mg) is the weight of the adsorbent.

2.4.2 Adsorption isotherms

SiO_2@IBR polymers (3 mg) were added to 3 mL TTX solution with initial concentrations of 6, 8, 10, 14, and 18 mg/L; the testing solution was placed in a shaker at 308 and 318 K. After being shaken for 720 min, the adsorbents were collected from the testing solution with tweezers, and squeezed until no solution could be expressed. Then the residual concentrations of TTX in solution were measured as shown in Section 2.4.1. The equilibrium adsorption capacity Q_e (mg/g) was calculated by (Xia et al., 2020)

$$Q_e=\frac{(C_0-C_e)\times V}{W}, \tag{3}$$

where Q_e (mg/g) is the equilibrium adsorption capacity; C_e (mg/L) is the equilibrium concentration of TTX.

2.4.3 Adsorption regeneration

SiO_2@IBR polymers (3 mg) were added to 3 mL of TTX solution with initial concentration of 10 mg/L. After being shaken for 720 min at 308 K, the adsorbents in the solution were collected with tweezers and squeezed until no solution could be expressed. Then the adsorbents were eluted with 0.1% (in volume) acetic acid solution (Su et al., 2010).

During the elution process, the adsorbents could also be squeezed to better elute the TTX. The above steps were repeated 10 times. Then, the residual concentrations of TTX in solution were measured as shown in Section 2.4.1.

3 Results and discussion

3.1 Characterization

3.1.1 Viscoelasticity and mechanical properties of IBR

The testing process and results for the viscoelasticity and other mechanical properties of IBR are illustrated in Fig. 2. The IBR was cut into two pieces; after reassembly and 24-h healing time, the pieces were firmly reconnected. We were able to stretch it to more than three times its original length before it broke again. After the pulling force was removed, the IBR completely returned to its original shape. The test results indicated that the bromine groups in BIIR reacted with primary and secondary amines through an N-alkylation reaction and successfully formed ionic imidazolium bromide groups, which significantly increased the viscosity of BIIR. The modified IBR had excellent viscoelasticity and mechanical properties, and was suitable for application in emulsions systems to prepare flexible materials with "shape-memory" functions.

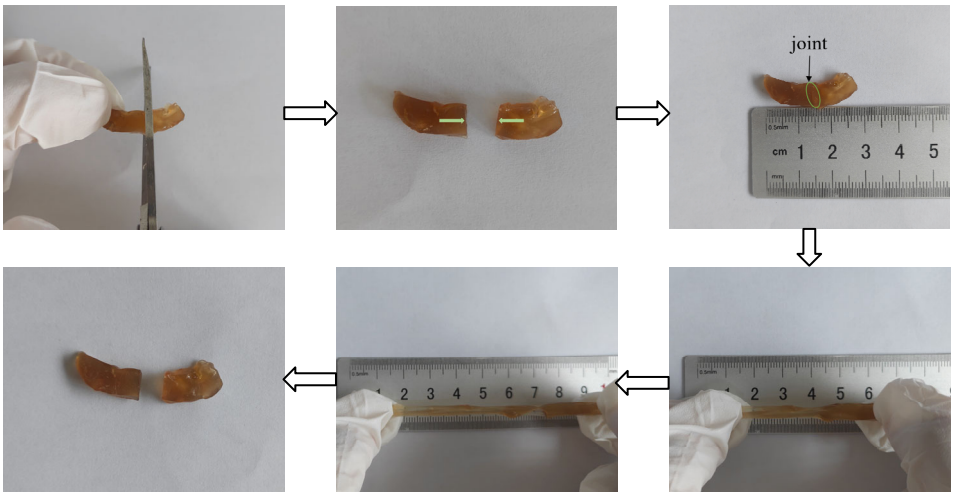

Fig. 2 Steps of the viscoelasticity and mechanical property tests

3.1.2 Morphology of Pickering O/W HIPEs

The illustration and experimental examples of SiO_2@IBR flexible shape-memory polymers prepared by Pickering O/W HIPEs polymerization are displayed in Fig. 3. As shown in Fig. 3a, when the outer (water) phase was combined with the inner (oil) phase, only a separation system was formed before stirring, and the SiO_2 nanoparticles were at the bottom of the sample bottle. The oil phase was added in small batches, and after the system was quickly stirred, the internal and external phases combined to form stable pale yellow Pickering O/W HIPEs. After 4 h, the emulsions were stable and no delamination occurred (Fig. 3c). An image of the emulsions under an optical microscope is shown in Fig. 3d. The prepared Pickering HIPEs had many large droplets, and the droplets were closely arranged. After the polymerization was initiated under high-temperature conditions, the polymers were observed to be pale yellow with many macroporous structures visible to the naked eye (Fig. 3e). The resultant polymers were pale yellow because there was a thin layer of rubber dispersed on the outer surface and pores, which connected the SiO_2 particles tightly.

The SEM images of SiO_2@IBR are shown in Fig. 4. The prepared SiO_2@IBR polymers were rich in pores and the macropores were above 200 μm in size. This kind of polymer material has interconnected macropores (Tan et al., 2018). An enlarged view of the inside of the aperture is shown in Fig. 4b, where regular and beautiful honeycomb structure can be seen. The honeycomb structure was like a fishing net, connecting SiO_2 particles in the mesh to protect them from falling off. At the same time, the honeycomb structure enhanced the mechanical properties, which was conducive to the adsorption and regeneration of the SiO_2@IBR (Chen et al., 2018; Lin et al., 2019).

3.1.3 FTIR

In this work, we applied ATR-FTIR spectra to determine the chemical composition of SiO_2@IBR before and after adsorption. As shown in Fig. 5, for

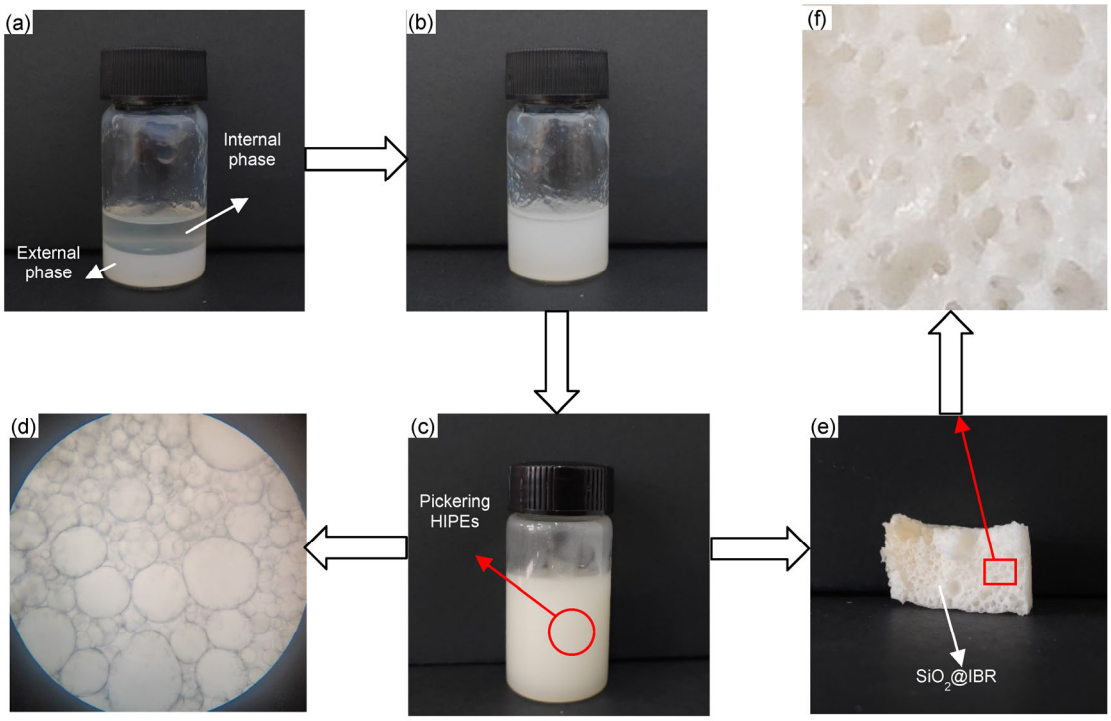

Fig. 3 Preparation of Pickering O/W HIPEs and SiO_2@IBR

(a) Phase-separated system; (b) Pickering emulsions formed after a small amount of oil phase was added for the first time; (c) Pickering O/W HIPEs; (d) Micrograph of the Pickering O/W HIPEs; (e) SiO_2@IBR flexible polymers; (f) Close-up of the SiO_2@IBR surface

the absorption curve of IBR, an absorption peak at 2950 cm^{-1} was attributed to the stretching vibration of $–CH_3$; absorption peaks near 2916 cm^{-1} and 2893 cm^{-1} were caused by the stretching vibration of $–CH_2$, and weaker double peaks located near 950 cm^{-1} and 923 cm^{-1} were caused by the shear vibration of $C═CH_2$ (Kotal et al., 2016). In the pre-adsorption SiO_2@IBR spectrum, a strong broad peak at 1085 cm^{-1} was associated with the stretching vibration of Si-O and an absorption peak at 1700 cm^{-1} was caused by the stretching vibration of C═O in –COOH in AA (Belgibayeva and Taniguchi, 2019; Lerma et al., 2020). The peaks corresponding to the IBR spectra appeared near 2950, 2916, 2893, 950, and 923 cm^{-1}, which showed that the SiO_2 and IBR were well combined and that the SiO_2@IBR polymer materials had been successfully prepared.

3.1.4 Shape-memory property

The SiO_2@IBR was nearly a cylinder, with a diameter of 19 mm and a height of 18 mm (Fig. 6). The compression test of SiO_2@IBR is shown in Fig. 7, and the relevant mechanical properties data are listed in Table 1. As shown in Fig. 7b, when the

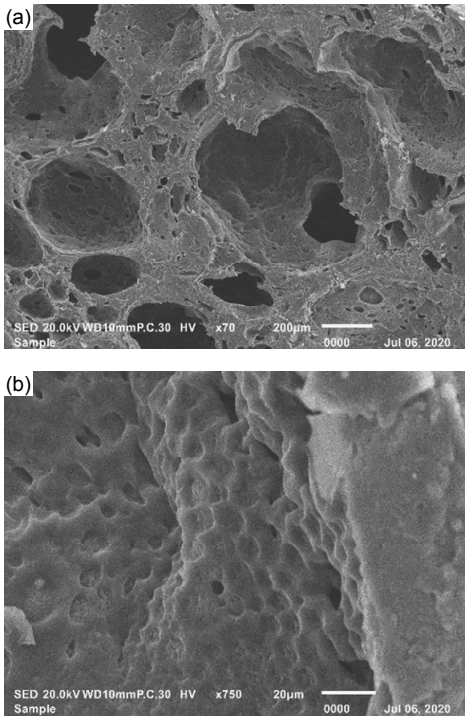

Fig. 4 SEM images of SiO_2@IBR at 200 μm (a) and 20 μm (b)

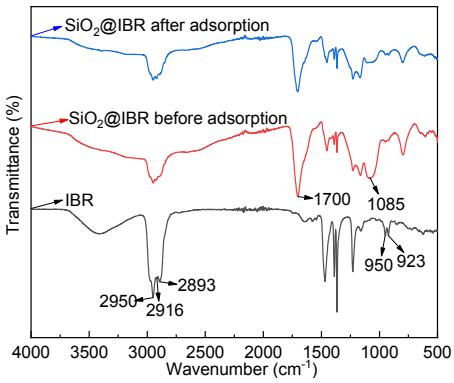

Fig. 5 FTIR spectra of IBR, SiO_2@IBR before adsorption, and SiO_2@IBR after adsorption

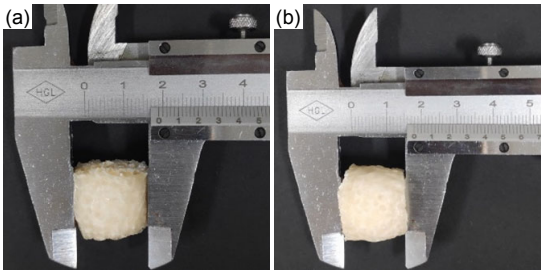

Fig. 6 SiO_2@IBR after drying: (a) diameter; (b) height

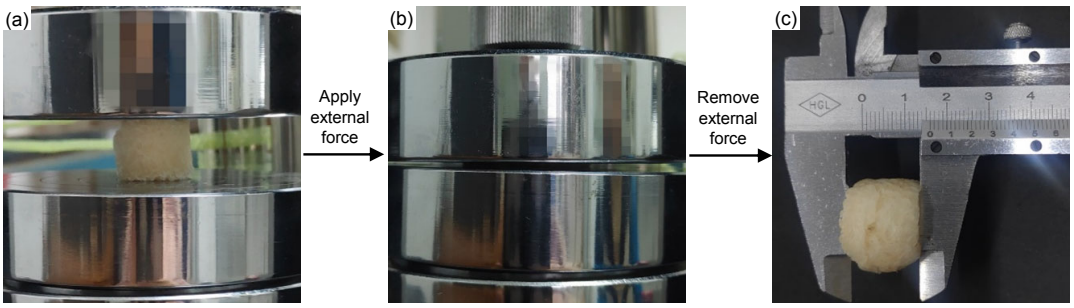

Fig. 7 Compression testing of SiO_2@IBR

(a) Before applying external force; (b) After applying external force; (c) After removing external force

maximum compression deformation was 16.10 mm, the deformation of the sample reached approximately 90%. When the pressure was removed, we observed that the sample was damaged to some extent, but it could still be restored to about 89% of the original height (Fig. 7c). The first two sets of data listed in Table 1 show that when the maximum compression deformation were 7.50 and 13.50 mm, the sample could basically be restored to its original height and no breakage was observed. This test proved that SiO_2@IBR had good shape memory. During the adsorption experiments, SiO_2@IBR could be continuously squeezed to remove the adsorbed TTX solution and eluent, allowing better adsorption and regeneration (Liu et al., 2016; Li et al., 2018).

3.1.5 Swelling property

The swelling test results are shown in Fig. 8. The water absorption rate of the samples increased rapidly at the beginning, slowed down after 60 min, and reached swelling equilibrium after 540 min. When the swelling equilibrium was reached, the water absorption rate was approximately 17.33 mg/mg. At that point, the weight of the samples was more than 18 times the original weight, and the volume was visibly larger.

Table 1 Basic parameters for numerical simulation

Order	Maximum load (N)	Compressive strength (MPa)	Maximum compression deformation (mm)
1	6.80	0.024	7.50
2	99.35	0.350	13.50
3	2953.80	10.418	16.10

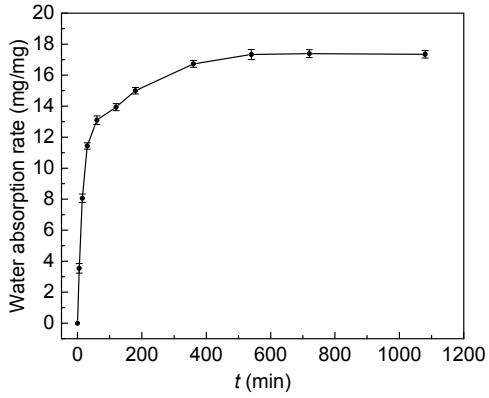

Fig. 8 Water absorption rate of SiO_2@IBR

Fig. 1S (can be found in the electronic supplementary materials) shows that during the swelling process, morphology changes in the samples corresponded to the water absorption rate. At the beginning, the samples swelled significantly, but they changed more slowly after 60 min, and almost stopped increasing in size around 540 min. When the swelling equilibrium was reached, the length of the samples had more than doubled. Thus, SiO_2@IBR had excellent water storage capacity and a relatively uniform water absorption rate; it could maintain a stable state after 18 h of soaking and still returned to the original state after drying. Therefore, it was evident that the pore structure of SiO_2@IBR was relatively uniform and firm, and that the pores were interconnected. Good pore connectivity and stable structure are important conditions for the application of macroporous materials in the field of adsorption (Qi et al., 2019, 2021). Consequently, we expect SiO_2@IBR to become a useful adsorbent material.

3.2 Adsorption experiments

3.2.1 Adsorption kinetics

Usually, adsorption kinetics and isotherms are used to study the adsorption performance of adsorbents. The adsorption kinetics data are particularly important for judging the equilibrium time and the binding mechanism (Zheng et al., 2016; Yao et al., 2019). We tested the kinetic performance of SiO_2@IBR when absorbing TTX at 308 K by kinetic experiments with different time intervals. The results are displayed in Fig. 9a. During the first 0–100 min, the adsorption capacity of SiO_2@IBR increased rapidly, but with time, it increased more slowly. After 200 min, the adsorption curve gradually became flat. The adsorption capacity Q_t of SiO_2@IBR at different times was calculated by Eq. (2). The specific nonlinear fitting equations were Eqs. (4) and (5). The initial adsorption rate h (mg/(g·min)) and half-equilibrium time $t_{1/2}$ (min) of SiO_2@IBR were calculated by Eqs. (6) and (7).

$$Q_t = Q_e - Q_e \cdot e^{-k_1 t}, \tag{4}$$

$$Q_t = \frac{k_2 Q_e^2 t}{1 + k_2 Q_e t}, \tag{5}$$

$$h = k_2 Q_e^2, \tag{6}$$

$$t_{1/2}=\frac{1}{k_2 Q_e}, \tag{7}$$

where k_1 (L/min) and k_2 (g/(mg·min)) are the respective rate constants associated with the pseudo-first-order and pseudo-second-order kinetics.

The fitting results of the two kinetic equations are shown in Table 2. Comparing the R^2 values, we found that both the quasi-first-order and quasi-second-order kinetic equations fitted the adsorption kinetic data well. The R^2 values were similar, and the fitting correlation of the quasi-second-order equation was slightly higher, indicating that the adsorption process involved chemical bonding accompanied by physical adsorption.

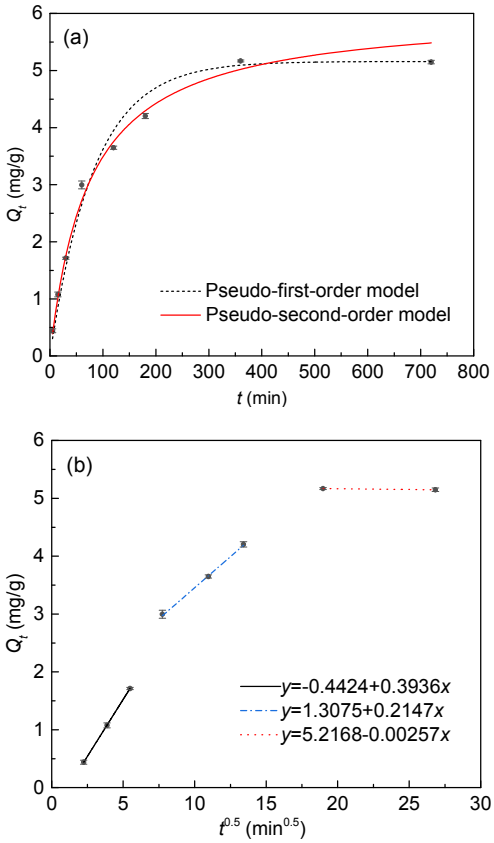

Fig. 9 Kinetic data and modeling for adsorption of TTX onto SiO_2@IBR (a) and intra-particle diffusion modeling for adsorption of TTX onto SiO_2@IBR (b)

At the same time, the kinetic data were fitted with an intra-particle diffusion model to clarify the diffusion mechanism in the process of TTX adsorption. The dynamic model formula proposed by Weber Jr and Morris (1963) is shown as

$$Q_t=K_{id}\cdot t^{0.5}+C, \tag{8}$$

where K_{id} (mg/(g·min$^{0.5}$)) is the intra-particle diffusion rate constant, and C is the constant representing the thickness of the boundary layer.

The fitting results of the intra-particle diffusion model are shown in Fig. 9b. The adsorption process can be divided into three stages. All three stages tended to be linear, but did not pass through the origin, which indicated that the adsorption process was jointly determined by multiple adsorption mechanisms (Karimi et al., 2019). The first stage was external surface adsorption. TTX molecules diffused into the macropores of SiO_2@IBR, and the adsorption capacity increased rapidly. Subsequently, in the second stage, TTX molecules diffused into the micropores of SiO_2@IBR and gradually reached an adsorption equilibrium state. The curve in the third stage was basically a straight horizontal line, indicating that the adsorption had reached equilibrium.

3.2.2 Adsorption isotherms

In addition, we studied the adsorption isotherm of SiO_2@IBR. The experimental results were fitted using Langmuir and Freundlich equivalent equations. The nonlinear fitting equations of the two models are Eqs. (9) and (10), respectively (Meng et al., 2013; Liu et al., 2011). The corresponding fitting data are illustrated in Table 3.

$$Q_e=\frac{Q_m K_L C_e}{1+K_L C_e}, \tag{9}$$

$$Q_m=K_F C_e^{1/n}, \tag{10}$$

where Q_m (mg/g) is the maximum adsorption capacity of SiO_2@IBR; K_L (L/mg) is the affinity constant of

Table 2 Kinetic model parameters obtained from adsorption of TTX onto SiO_2@IBR

Temperature (K)	Pseudo-first-order equation			Pseudo-second-order equation		
	Q_e (mg/g)	k_1 (L/min)	R^2	Q_e (mg/g)	k_2 (g/(mg·min))	R^2
308	5.15	0.0120	0.988	6.04	0.0022	0.991

the Langmuir isotherm; K_F (mg/g) is the adsorption equilibrium constant of the Freundlich isotherm; $1/n$ is a measure of exchange intensity or surface heterogeneity, with a value of $1/n$ less than 1.0, describing a favorable removal condition.

The separation factor R_L was used to analyze the advantages of adsorption, which can be given by

$$R_L=\frac{1}{1+C_mK_L}, \tag{11}$$

where C_m (mg/L) is the maximum initial concentration of TTX.

According to the curves shown in Fig. 10, the isotherm of SiO_2@IBR always has a rapid growth trend, which is probably because the TTX concentrations in the experiment were relatively low.

As can be seen from Table 3, the data were fitted well by the Langmuir and Freundlich isotherm models. The R^2 values were very similar. At 308 and 318 K, the values for $1/n$ were 0.986 and 0.980, respectively; the fact that these were both less than 1 indicates that the adsorption conditions were beneficial to controlling the adsorption of TTX onto the adsorbent, and the adsorption of TTX was monolayer.

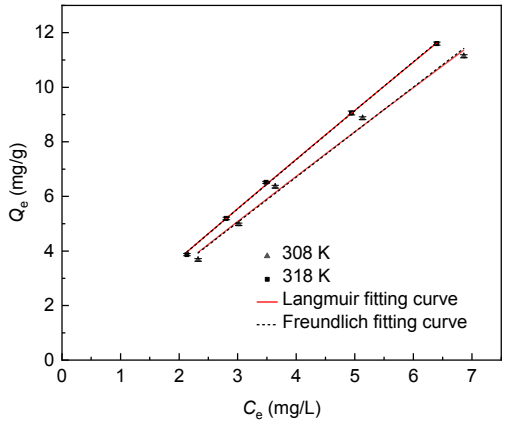

Fig. 10 Equilibrium data and modeling for adsorption of TTX onto SiO_2@IBR

The adsorption process of SiO_2@IBR to TTX was chemical adsorption accompanied by physical adsorption, and the adsorption mechanism was complicated. For the physical adsorption process, the possible forms are hydrogen bonding, a π-π effect, an electrostatic effect, and van der Waals forces. The main interaction between SiO_2 nanoparticles and TTX was electrostatic, and the negative surface had a great affinity for compounds with positive charges (Liu et al., 2020). In the spectrum of SiO_2@IBR after adsorption, the intensity of the 1085 cm^{-1} broad peak was obviously weakened, which may have been caused by this electrostatic effect (Fig. 6). The peak intensity of –COOH at 1700 cm^{-1} was also significantly weakened, due to the participation of –COOH in chemical adsorption. The adsorption mechanism is shown in Fig. 11. Under neutral conditions, TTX may appear as $C_{11}H_{16}O_8N_2NH_2^+$. Essentially, –COOH ionized H^+ in the water and exchanged with $C_{11}H_{16}O_8N_2NH_2^+$, which was abundant in the solution, so that TTX was adsorbed on SiO_2@IBR (Zhao et al., 2019).

3.2.3 Adsorption regeneration

In order to test regeneration capacity, we performed 10 consecutive adsorption-regeneration cycle experiments on SiO_2@IBR. As shown in Fig. 12, compared with the first test, the adsorption capacity in the second test did not decrease but increased. The possible reason is that after an adsorption-desorption experiment on the SiO_2@IBR adsorbent, some

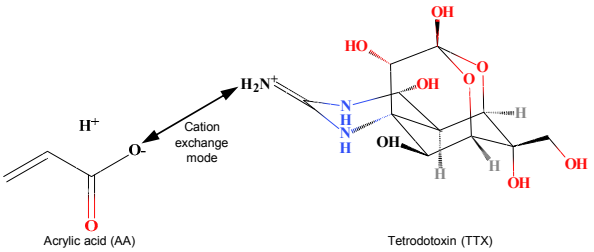

Fig. 11 Schematic diagram of the chemical adsorption mechanism of TTX

Table 3 Fitting parameters of the Langmuir and Freundlich equations for TTX adsorption onto SiO_2@IBR

T (K)	Langmuir isotherm equation				Freundlich isotherm equation		
	Q_m (mg/g)	K_L (L/min)	R_L	R^2	K_F (mg/g)	$1/n$	R^2
308	290.44	0.0059	0.90	0.9888	1.70	0.986	0.9881
318	338.12	0.0055	0.91	0.9989	1.88	0.980	0.9987

blockage in its pores was opened, providing more adsorption sites. After 10 cycles of regeneration experiments, the adsorption capacity decreased less than 0.03%. The results suggested that the SiO_2@IBR flexible polymers introduced with IBR rubber as adsorbent materials are suitable to be recycled repeatedly; they had excellent regeneration ability, and their adsorption performance was resilient to operations such as desorption, washing, and drying.

Even after SiO_2@IBR was adsorbed, swelled, desorbed, and washed, the SiO_2 particles were closely pulled together under the combined action of cross-linking polymerization and IBR. After drying, the SiO_2 particles were still tightly linked, preventing the material from being lost. In general, due to its good mechanical tensile properties and macroporous properties, SiO_2@IBR has excellent regeneration cycle capabilities. Table 4 summarizes the adsorption regeneration performance of various adsorbents reported in the literature. Compared with the three nanocomposites reported by Tanzifi et al. (2018a) and Tanzifi et al. (2018b) (within five cycles), the adsorption capacity reduction rate of SiO_2@IBR is much smaller, proving that making nanoparticles into polymers is beneficial to the recycling of adsorbents. Compared with the two polymers prepared by Safi et al. (2019) and Sun et al. (2020) (within seven cycles), after seven adsorption regeneration experiments, the regeneration efficiency of SiO_2@IBR was higher at 98.9%, confirming that the introduction of IBR had a positive effect on the regeneration efficiency of the adsorbent.

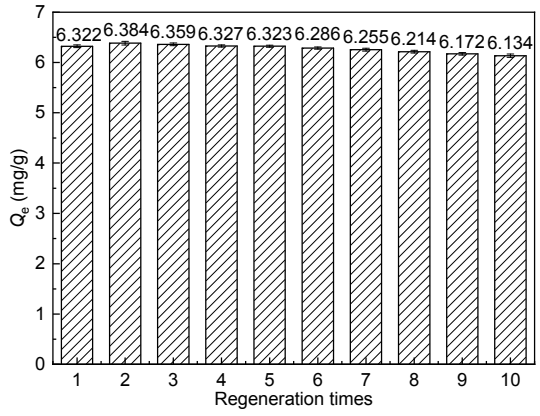

Fig. 12 Regeneration of SiO_2@IBR for 10 cycles

4 Conclusions

We prepared flexible shape-memory polymers (SiO_2@IBR) by Pickering HIPE polymerization, and applied them for the adsorption and separation of TTX. The successful formation of the SiO_2@IBR polymers was characterized with various methods which showed that the polymers had well-defined macroporous structure and good flexibility. The particular shape memory of SiO_2@IBR is beneficial to the adsorption and regeneration process. Batches of adsorption experiments proved that SiO_2@IBR is an effective and promising adsorbent with good adsorption capacity for TTX. Both the Langmuir and Freundlich models accurately describe the isothermal adsorption data. The results of the pseudo-first-order and pseudo-second-order kinetic models indicated that there was chemical bonding accompanied by physical adsorption. The regeneration experiments results demonstrated that SiO_2@IBR has good adsorption regeneration performance. After 10 regeneration experiments, the adsorption capacity decreased less than 0.03%. Therefore, SiO_2@IBR polymers have potential for adsorption and separation, and will be valuable for the development of new separation and extraction methods.

Table 4 Adsorption regeneration properties of some adsorbents reported in the literature

Adsorbent	Target	Reduction of adsorption capacity	Reference
Polyaniline/SiO_2 nanocomposite	Amido Black 10B	99%→84.5%	Tanzifi et al., 2018a
Polyaniline/carboxymethyl cellulose/TiO_2 nanocomposites	Dye	98.82%→95.86%	Tanzifi et al., 2018b
Polypyrrole/CMC composite nanoparticles	Reactive dyes	RR56: 93.46%→84.8%; RB160: 94.05%→85.4%	Tanzifi et al., 2020
Gel composite	Arsenic	Regeneration efficiency 87.6%	Safi et al., 2019
SiO_2@ZIF-67/CNTs	Methyl orange	Regeneration efficiency 90.0%	Sun et al., 2020
SiO_2@IBR	TTX	Regeneration efficiency 97.0%	This work

CMC: carboxymethyl cellulose; ZIF: zeoliticimidazolate frameworks; CNTs: carbon nanotubes

Contributors

Hong-xiang OU provided research direction, gave help in the experiments, and participated in the revision of the paper. Chen-xia GONG formulated the experimental plan, completed a series of experiments, processed the experimental data, and wrote and revised the paper. Hong-lai XUE participated in the paper revision. Dong-sheng ZHOU and Kai-jia LI assisted in some experiments. Shu-cheng LIU gave some technical support to the problems that occurred during the experiments.

Conflict of interest

Hong-xiang OU, Chen-xia GONG, Hong-lai XUE, Dong-sheng ZHOU, Kai-jia LI, and Shu-cheng LIU declare that they have no conflict of interest.

References

Azhar U, Huo ZY, Yaqub R, et al., 2019. Non-crosslinked fluorinated copolymer particles stabilized Pickering high internal phase emulsion for fabrication of porous polymer monoliths. *Polymer*, 172:160-169. https://doi.org/10.1016/j.polymer.2019.03.068

Belgibayeva A, Taniguchi I, 2019. Synthesis and characterization of SiO_2/C composite nanofibers as free-standing anode materials for Li-ion batteries. *Electrochimica Acta*, 328:135101. https://doi.org/10.1016/j.electacta.2019.135101

Chen J, Zhu JW, Wang N, et al., 2019. Hydrophilic polythiophene/SiO_2 composite for adsorption engineering: green synthesis in aqueous medium and its synergistic and specific adsorption for heavy metals from wastewater. *Chemical Engineering Journal*, 360:1486-1497. https://doi.org/10.1016/j.cej.2018.10.228

Chen WZ, Xie QL, Zhang YP, et al., 2014. Development of anhydrotetrodotoxin certiifed reference material. *Chemical Analysis and Meterage*, 23(3):1-4 (in Chinese). https://doi.org/10.3969/j.issn.1008-6145.2014.03.001

Chen X, Xu Y, Liang MM, et al., 2018. Honeycomb-like polysulphone/polyurethane nanofiber filter for the removal of organic/inorganic species from air streams. *Journal of Hazardous Materials*, 347:325-333. https://doi.org/10.1016/j.jhazmat.2018.01.012

Chen YR, Cheng J, 1984. Quantitative determination of tetrodotoxin by ultraviolet spectrophotometry. *Chinese Journal of Marine Drugs*, (2):9-11 (in Chinese).

Cheng S, Liu XM, Zhen JH, et al., 2019. Preparation of superabsorbent resin with fast water absorption rate based on hydroxymethyl cellulose sodium and its application. *Carbohydrate Polymers*, 225:115214. https://doi.org/10.1016/j.carbpol.2019.115214

Das A, Sallat A, Böhme F, et al., 2015. Ionic modification turns commercial rubber into a self-healing material. *ACS Applied Materials & Interfaces*, 7(37):20623-20630. https://doi.org/10.1021/acsami.5b05041

Das AB, Goud VV, Das C, 2018. Adsorption/desorption, diffusion, and thermodynamic properties of anthocyanin from purple rice bran extract on various adsorbents. *Journal of Food Process Engineering*, 41(6):e12834. https://doi.org/10.1111/jfpe.12834

Deniz Akbora H, Kunter İ, Erçetin T, et al., 2020. Determination of tetrodotoxin (TTX) levels in various tissues of the silver cheeked puffer fish (*Lagocephalus sceleratus* (Gmelin, 1789)) in Northern Cyprus Sea (Eastern Mediterranean). *Toxicon*, 175:1-6. https://doi.org/10.1016/j.toxicon.2019.12.002

Dupont H, Fouché C, Dourges MA, et al., 2020. Polymerization of cellulose nanocrystals-based Pickering HIPE towards green porous materials. *Carbohydrate Polymers*, 243:116411. https://doi.org/10.1016/j.carbpol.2020.116411

Fan Y, Zhang Y, Peng C, et al., 2020. Preparation of teamed boronate affinity magnetic nanoparticles for extraction of polyphenols from flos lonicerae beverage under neutral pH prior to their determination by high-performance liquid chromatography-mass spectrometry. *Journal of Chromatography A*, 1619:460913. https://doi.org/10.1016/j.chroma.2020.460913

Hagen NA, Cantin L, Constant J, et al., 2017. Tetrodotoxin for moderate to severe cancer-related pain: a multicentre, randomized, double-blind, placebo-controlled, parallel-design trial. *Pain Research and Management*, 2017: 7212713. https://doi.org/10.1155/2017/7212713

Hong BH, He JL, Le QQ, et al., 2019. Combination formulation of tetrodotoxin and lidocaine as a potential therapy for severe arrhythmias. *Marine Drugs*, 17(12):685. https://doi.org/10.3390/md17120685

Huang ZM, Liu ZY, Su J, et al., 2011. Study on ultrasonic-assisted extraction of tetrodotoxin. *Journal of Guangdong Ocean University*, 31(6):79-85 (in Chinese). https://doi.org/10.3969/j.issn.1673-9159.2011.06.013

Kan LL, Guo B, 2008. Research on the ultrasonic extraction of TTX by orthogonal design. *Chinese Archives of Traditional Chinese Medicine*, 26(6):1274-1275 (in Chinese). https://doi.org/10.3969/j.issn.1673-7717.2008.06.063

Karimi S, Yaraki MT, Karri RR, 2019. A comprehensive review of the adsorption mechanisms and factors influencing the adsorption process from the perspective of bioethanol dehydration. *Renewable and Sustainable Energy Reviews*, 107:535-553. https://doi.org/10.1016/j.rser.2019.03.025

Kotal M, Banerjee SS, Bhowmick AK, 2016. Functionalized graphene with polymer as unique strategy in tailoring the properties of bromobutyl rubber nanocomposites. *Polymer*, 82:121-132. https://doi.org/10.1016/j.polymer.2015.11.044

Lerma TA, Garcés V, Palencia M, 2020. Novel multi- and bio-functional hybrid polymer hydrogels based on bentonite-poly(acrylic acid) composites and sorbitol polyesters: structural and functional characterization. *European Polymer Journal*, 128:109627. https://doi.org/10.1016/j.eurpolymj.2020.109627

Li J, Zuo KM, Wu WB, et al., 2018. Shape memory aerogels from nanocellulose and polyethyleneimine as a novel

adsorbent for removal of Cu(II) and Pb(II). *Carbohydrate Polymers*, 196:376-384. https://doi.org/10.1016/j.carbpol.2018.05.015

Li WJ, Dong XL, Zhu LH, et al., 2020. Highly selective separation of Re(VII) from Mo(VI) by using biomaterial-based ionic gel adsorbents: extractive adsorption enrichment of Re and surface blocking of Mo. *Chemical Engineering Journal*, 387:124078. https://doi.org/10.1016/j.cej.2020.124078

Lin DC, Shi M, Wei XX, et al., 2019. Development of an innovative capsule with three-dimension honeycomb architecture via one-step titration-gel method for the removal of methylene blue. *International Journal of Biological Macromolecules*, 128:911-922. https://doi.org/10.1016/j.ijbiomac.2019.02.001

Liu Q, Liu Y, Zhang ZH, et al., 2020. Adsorption of cationic dyes from aqueous solution using hydrophilic silica aerogel via ambient pressure drying. *Chinese Journal of Chemical Engineering*, 28(9):2467-2473. https://doi.org/10.1016/j.cjche.2020.04.023

Liu SC, Pan JM, Cao J, et al., 2016. Simultaneous removal of Pb(II) and 2,4,6-trichlorophenol by a hierarchical porous PU@PDA@MSNs sponge with reversible "shape memory" effect. *Chemical Engineering Journal*, 284: 10-20. https://doi.org/10.1016/j.cej.2015.08.133

Liu Y, Liu ZC, Gao J, et al., 2011. Selective adsorption behavior of Pb(II) by mesoporous silica SBA-15-supported Pb(II)-imprinted polymer based on surface molecularly imprinting technique. *Journal of Hazardous Materials*, 186(1):197-205. https://doi.org/10.1016/j.jhazmat.2010.10.105

Lu TT, Zhu YF, Wang WB, et al., 2019. Interconnected superporous adsorbent prepared via yeast-based Pickering HIPEs for high-efficiency adsorption of Rb^+, Cs^+ and Sr^{2+}. *Chemical Engineering Journal*, 361:1411-1422. https://doi.org/10.1016/j.cej.2018.11.006

Meng MJ, Feng YH, Zhang M, et al., 2013. Optimization of surface imprinted layer attached poly(vinylidene fluoride) membrane for selective separation of salicylic acid from acetylsalicylic acid using central composite design. *Chemical Engineering Journal*, 231:132-145. https://doi.org/10.1016/j.cej.2013.07.015

Ohyabu N, Nishikawa T, Isobe M, 2003. First asymmetric total synthesis of tetrodotoxin. *Journal of the American Chemical Society*, 125(29):8798-8805. https://doi.org/10.1021/ja0342998

Peng YT, Shen Y, Ge MY, et al., 2019. Efficient extraction of heavy metals from collagens by sulfonated polystyrene nanospheres. *Food Chemistry*, 275:377-384. https://doi.org/10.1016/j.foodchem.2018.09.111

Pichierri F, 2016. Molecular structures of two tetrodotoxin analogs containing a monooxa-hydrocarbon cage: a computational study. *Journal of Molecular Structure*, 1106:407-415. https://doi.org/10.1016/j.molstruc.2015.11.006

Qi XL, Chen MY, Qian YN, et al., 2019. Construction of macroporous salecan polysaccharide-based adsorbents for wastewater remediation. *International Journal of Biological Macromolecules*, 132:429-438. https://doi.org/10.1016/j.ijbiomac.2019.03.155

Qi XL, Zeng QK, Tong XQ, et al., 2021. Polydopamine/montmorillonite-embedded pullulan hydrogels as efficient adsorbents for removing crystal violet. *Journal of Hazardous Materials*, 402:123359. https://doi.org/10.1016/j.jhazmat.2020.123359

Rattanasom N, Prasertsri S, Suchiva K, 2009. Mechanical properties, thermal stability, gas permeability, and phase morphology in natural rubber/bromobutyl rubber blends. *Journal of Applied Polymer Science*, 113(6):3985-3992. https://doi.org/10.1002/app.30451

Safi SR, Gotoh T, Iizawa T, et al., 2019. Development and regeneration of composite of cationic gel and iron hydroxide for adsorbing arsenic from ground water. *Chemosphere*, 217:808-815. https://doi.org/10.1016/j.chemosphere.2018.11.050

Segiet D, Neuendorf LM, Tiller JC, et al., 2020. Realizing a shape-memory effect for synthetic rubber (IR). *Polymer*, 203:122788. https://doi.org/10.1016/j.polymer.2020.122788

Song H, li J, Lu CL, et al., 2011. Tetrodotoxin alleviates acute heroin withdrawal syndrome: a multicentre, randomized, double-blind, placebo-controlled study. *Clinical and Experimental Pharmacology and Physiology*, 38(8):510-514. https://doi.org/10.1111/j.1440-1681.2011.05539.x

Su J, Liu ZY, Huang ZM, 2010. A research on tetrodotoxin purification. *Journal of Fujian Fisheries*, (4):56-59 (in Chinese). https://doi.org/10.3969/j.issn.1006-5601.2010.04.012

Sun HM, Ju CG, Zhao YW, et al., 2020. Preparation of SiO_2@ZIF-67/CNTs and research on its adsorption performance at low-temperature. *Colloids and Surfaces A: Physicochemical and Engineering Aspects*, 603:125205. https://doi.org/10.1016/j.colsurfa.2020.125205

Tan HT, Tu SH, Zhao YL, et al., 2018. A simple and environment-friendly approach for synthesizing macroporous polymers from aqueous foams. *Journal of Colloid and Interface Science*, 509:209-218. https://doi.org/10.1016/j.jcis.2017.09.018

Tanzifi M, Tavakkoli Yaraki M, Kiadehi AD, et al., 2018a. Adsorption of Amido Black 10B from aqueous solution using polyaniline/SiO_2 nanocomposite: experimental investigation and artificial neural network modeling. *Journal of Colloid and Interface Science*, 510:246-261. https://doi.org/10.1016/j.jcis.2017.09.055

Tanzifi M, Tavakkoli Yaraki M, Karami M, et al., 2018b. Modelling of dye adsorption from aqueous solution on polyaniline/carboxymethyl cellulose/TiO_2 nanocomposites. *Journal of Colloid and Interface Science*, 519: 154-173. https://doi.org/10.1016/j.jcis.2018.02.059

Tanzifi M, Tavakkoli Yaraki M, Beiramzadeh Z, et al., 2020. Carboxymethyl cellulose improved adsorption capacity of polypyrrole/CMC composite nanoparticles for removal of reactive dyes: experimental optimization and DFT calculation. *Chemosphere*, 255:127052. https://doi.org/10.1016/j.chemosphere.2020.127052

Wang B, Chen PY, Zhao RX, et al., 2020. Carbon-dot modified polyacrylonitrile fibers: recyclable materials capable of selectively and reversibly adsorbing small-sized anionic dyes. *Chemical Engineering Journal*, 391:123484. https://doi.org/10.1016/j.cej.2019.123484

Wang QZ, Qin Y, Xue CL, et al., 2020. Facile fabrication of bubbles-enhanced flexible bioaerogels for efficient and recyclable oil adsorption. *Chemical Engineering Journal*, 402:126240. https://doi.org/10.1016/j.cej.2020.126240

Weber Jr WJ, Morris JC, 1963. Closure to "kinetics of adsorption on carbon from solution". *Journal of the Sanitary Engineering Division*, 89(2):53-55. https://doi.org/10.1061/JSEDAI.0000467

Xia Y, Zhou JJ, Gong YY, et al., 2020. Strong influence of surfactants on virgin hydrophobic microplastics adsorbing ionic organic pollutants. *Environmental Pollution*, 265:115061. https://doi.org/10.1016/j.envpol.2020.115061

Yang F, Jing DT, Yu DW, et al., 2019. Differential roles of ice crystal, endogenous proteolytic activities and oxidation in softening of obscure pufferfish (*Takifugu Obscurus*) fillets during frozen storage. *Food Chemistry*, 278:452-459. https://doi.org/10.1016/j.foodchem.2018.11.084

Yao JT, Ma Y, Liu JX, et al., 2019. Janus-like boronate affinity magnetic molecularly imprinted nanobottles for specific adsorption and fast separation of luteolin. *Chemical Engineering Journal*, 356:436-444. https://doi.org/10.1016/j.cej.2018.09.003

Yi WY, Wu H, Wang HT, et al., 2016. Interconnectivity of macroporous hydrogels prepared via graphene oxide-stabilized Pickering high internal phase emulsions. *Langmuir*, 32(4):982-990. https://doi.org/10.1021/acs.langmuir.5b04477

Zhang NL, Wang WL, Li B, et al., 2019. Non-volatile taste active compounds and umami evaluation in two aquacultured pufferfish (*Takifugu obscurus* and *Takifugu rubripes*). *Food Bioscience*, 32:100468. https://doi.org/10.1016/j.fbio.2019.100468

Zhao LQ, Chen JX, Xiong N, et al., 2019. Carboxylation as an effective approach to improve the adsorption performance of graphene materials for Cu^{2+} removal. *Science of the Total Environment*, 682:591-600. https://doi.org/10.1016/j.scitotenv.2019.05.190

Zheng XD, Liu EL, Zhang FS, et al., 2016. Efficient adsorption and separation of dysprosium from NdFeB magnets in an acidic system by ion imprinted mesoporous silica sealed in a dialysis bag. *Green Chemistry*, 18(18):5031-5040. https://doi.org/10.1039/C6GC01426G

List of electronic supplementary materials

Fig. S1 Morphology changes during the swelling process of SiO_2@IBR